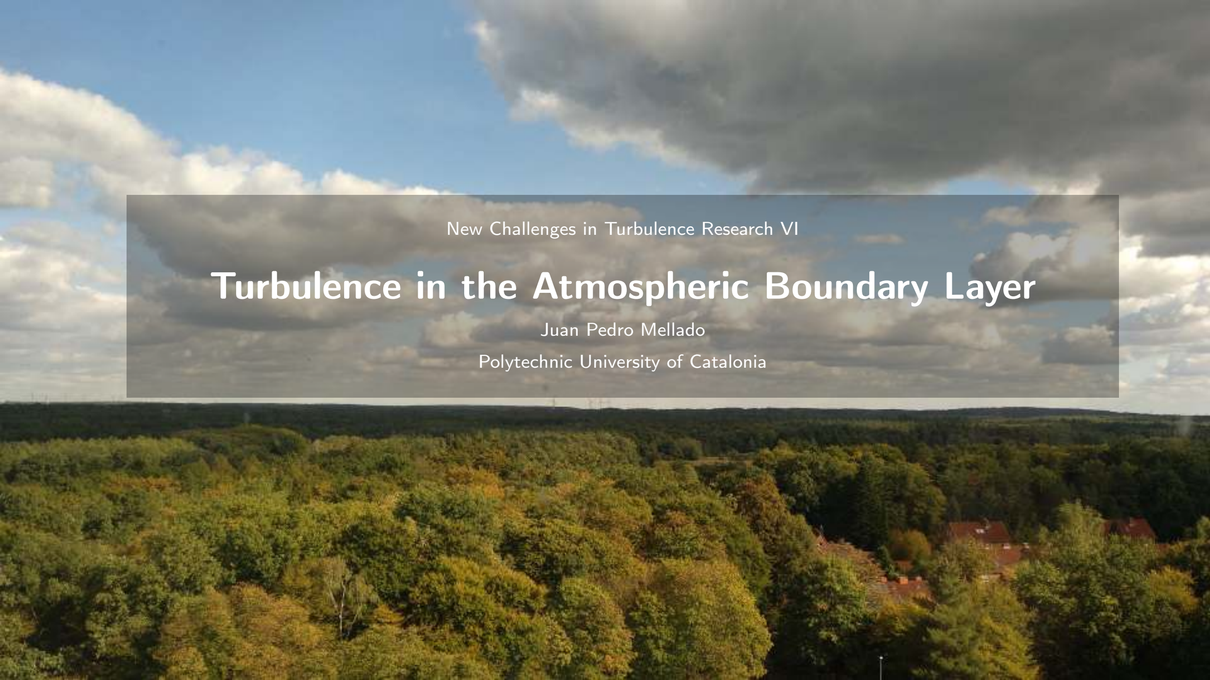

New Challenges in Turbulence Research VI

Turbulence in the Atmospheric Boundary Layer

Juan Pedro Mellado

Polytechnic University of Catalonia

The Atmospheric Boundary Layer (ABL)

The ABL is the lower layer of the atmosphere, the layer that reacts to surface phenomena on time scales shorter than a day. Its depth varies between a few hundred meters to $2 - 3\ \mathrm{km}$.

Normally turbulent, because of wind shear or because of convection.

Lüneburg, Germany.

The Atmospheric Boundary Layer (ABL)

The ABL is the lower layer of the atmosphere, the layer that reacts to surface phenomena on time scales shorter than a day. Its depth varies between a few hundred meters to $2 - 3\ \mathrm{km}$.

Normally turbulent, because of wind shear or because of convection.

North Atlantic. Courtesy of Cedrick Ansorge.

The Atmospheric Boundary Layer (ABL)

The ABL is the lower layer of the atmosphere, the layer that reacts to surface phenomena on time scales shorter than a day. Its depth varies between a few hundred meters to $2-3\ \mathrm{km}$.

Normally turbulent, because of wind shear or because of convection.

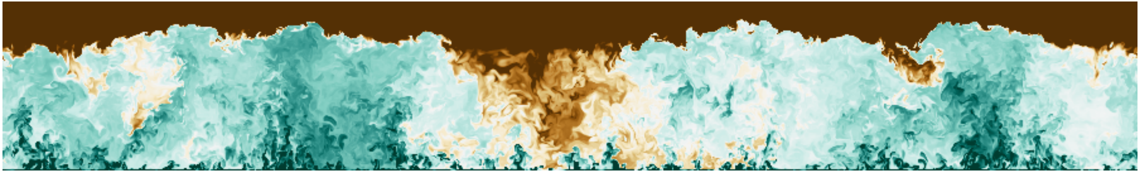

Moisture field from DNS at Reynolds number 10^4 (1000 m deep ABL resolved to 2 m)

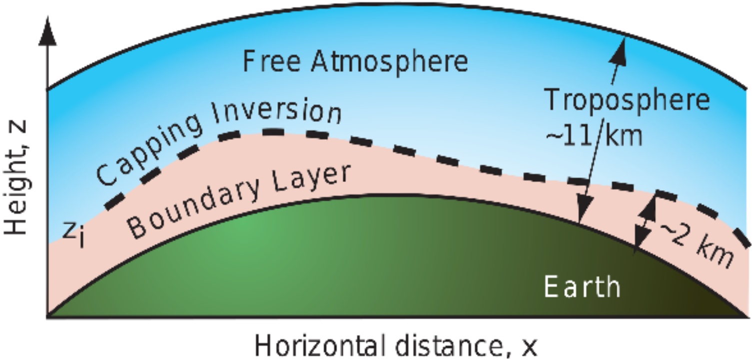

- We live in the ABL: important for energy, transportation, pollution, agriculture.
- Important for climate: the ABL modulates the fluxes between the atmosphere, land and ocean.

Wyngaard [2010]. Figure 9.1 from Wallace and Hobbs [2006].

Importance and Challenges

Importance for Climate and Weather Models

- Long-standing biases in weather and climate models are often rooted in the ABL.

  Reynolds et al. [2019], LeMone et al. [2019]

- Kilometer-scale resolution will require re-evaluation of parametrizations.

  Stevens and et. al. [2019]

Importance and Challenges

Importance for Climate and Weather Models

- Long-standing biases in weather and climate models are often rooted in the ABL.
  Reynolds et al. [2019], LeMone et al. [2019]
- Kilometer-scale resolution will require re-evaluation of parametrizations.
  Stevens and et. al. [2019]

Challenges

Multiscale | Multiphysics | Variability | Data

- meter and submeter scales can affect mesoscale and larger properties and dynamics,
- turbulence is not alone,
- different regimes and transients induced by diurnal cycle and mesoscale conditions,
- we need accurate data that simultaneously covers various processes at various scales.

Multi-Scale

ABL depths of $1\ \mathrm{km}$ and velocity fluctuations of $1\ \mathrm{m\ s^{-1}}$ yield a Reynolds number 10^8 and a length scale ratio of large energy containing motions to small dissipative ones of 10^6.

Turbulence tends to organize into large-scale motions and is strongly inhomogeneous.

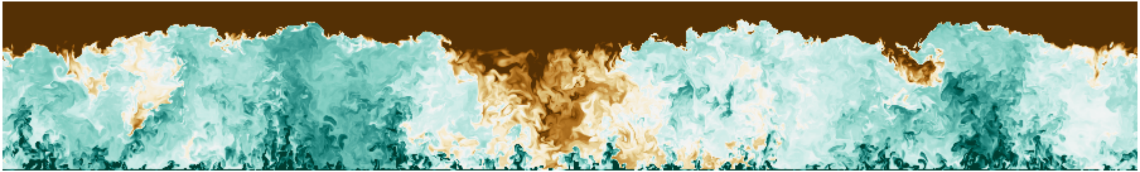

Moisture field from DNS at Reynolds number 10^4 (1000 m deep ABL resolved to 2 m)

Large scales generally dominate vertical mixing, but small scales (meter, submeter) become important

- near the surface, where density stratification or heterogeneity can change global properties,
- near the ABL top, where stratification and clouds can alter entrainment and radiative transfer,
- for cloud dynamics, precipitation, cold pools, ...

Challenges Associated with Turbulence

- stably stratified turbulence and turbulence–gravity-wave interaction
- near-surface turbulence, effect of surface roughness and surface heterogeneity
- large coherent motions (convection cells, rolls) and their interaction with the small scales
- statistical heterogeneity, as induced by organization or by strong mean vertical gradients near the surface or near the ABL top,
- history effects in Lagrangian properties or mixing,
- statistical anisotropy, such as temperature fronts, or strongly stratified regions,
- external intermittency, such as at the ABL top or during turbulence collapse in stable ABLs.

Multi-Physics

- Turbulence and mixing.
  Shear driven, buoyancy driven, stratified, wall bounded, wall free, entrainment, dispersion...

  But turbulence is not alone, there is a complex process interaction with

- Cloud physics.
  Latent heat effects, microphysics (liquid and ice).
- Radiative transfer.
  Longwave outgoing radiation, shortwave incoming radiation.
- Chemistry, aerosols.
  Pollution, nucleation of cloud particles.
- Surface processes.
  Surface energy balance, heterogeneity, roughness, ocean-atmosphere interaction.

Each bullet is a field of research, but interdisciplinarity is needed.

Turbulence in the Atmospheric Boundary Layer

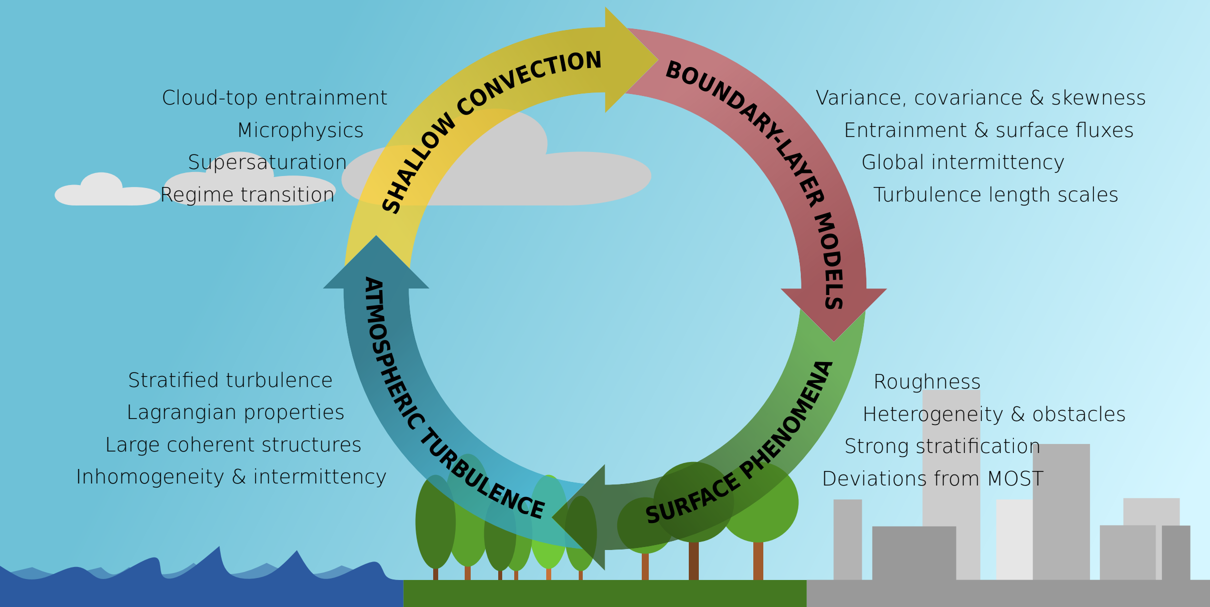

$$
\begin{aligned}
&\rho\mathbf{v}) = 0 \\
&\mathbf{v}) = -\nabla p + \nabla\cdot\boldsymbol{\tau} + \rho\mathbf{g} \\
&e_\mathrm{k}) = -\nabla\cdot(\rho\mathbf{j}_h + \rho\mathbf{j}_r - \\
&)q_\mathrm{v} = -\nabla\cdot(\rho\mathbf{j}_\mathrm{v}) \ ,
\end{aligned}
$$

Contents

Conservation Equations in a Cloud-Free Atmosphere

$$\partial_t \rho + \nabla\cdot(\rho \mathbf{v}) = 0 \tag{1a}$$

$$\rho(\mathrm{D}\mathbf{v} + 2\boldsymbol{\Omega} \times \mathbf{v}) = -\nabla p + \nabla\cdot\boldsymbol{\tau} + \rho\mathbf{g} \tag{1b}$$

$$\rho\mathrm{D}(h + e_\mathrm{p} + e_\mathrm{k}) = -\nabla\cdot(\rho\mathbf{j}_h + \rho\mathbf{j}_r - \boldsymbol{\tau}\cdot\mathbf{v}) + \partial_t p\ , \tag{1c}$$

$$\rho\mathrm{D}q_\mathrm{v} = -\nabla\cdot(\rho\mathbf{j}_\mathrm{v})\ , \tag{1d}$$

where

- $\boldsymbol{\Omega}$ is the angular velocity of the frame of reference,
- $\mathbf{g}$ is the gravitational acceleration, assumed constant.
- $e_\mathrm{p} = gz$ is the potential energy per unit mass, and $e_\mathrm{k} = v^2/2$ is the kinetic energy.
- $\mathbf{j}_r$ is the flux of radiative energy.
- h is the enthalpy of the mixture of water vapor and dry air.
- q_v is the water-vapor specific humidity, the mass of water vapor per unit mass of the **mixture of water vapor and dry air**. Typical values are $q_\mathrm{v} \approx 1 - 10\ \mathrm{g\ kg}^{-1}$.
  $q_\mathrm{d} = 1 - q_\mathrm{v}$ is the mass fraction of dry air.
  (The mixing ratio r_v, the mass of water vapor per unit mass of dry air, is also used.)

Anelastic Approximation

Decompose the thermodynamic state of a fluid particle into a reference state that describes a **hydrostatic base-state** atmosphere,

$$\nabla p_{\mathrm{ref}} = \rho_{\mathrm{ref}} \mathbf{g} \,, \tag{2}$$

and a deviation thereof, e.g., $\rho'(\mathbf{x},t) \equiv \rho(\mathbf{x},t) - \rho_{\mathrm{ref}}(z)$, $p'(\mathbf{x},t) \equiv p(\mathbf{x},t) - p_{\mathrm{ref}}(z)$, ...

Assumptions:

1. Deviations are small.
2. Mach number is small.
3. hydrostatic base-state is close to isentropic state.
4. hydrostatic base-state is quasi-steady.

Anelastic Approximation

Decompose the thermodynamic state of a fluid particle into a reference state that describes a **hydrostatic base-state** atmosphere,

$$\nabla p_{\mathrm{ref}} = \rho_{\mathrm{ref}}\mathbf{g} \; , \tag{2}$$

and a deviation thereof, e.g., $\rho'(\mathbf{x}, t) \equiv \rho(\mathbf{x}, t) - \rho_{\mathrm{ref}}(z)$, $p'(\mathbf{x}, t) \equiv p(\mathbf{x}, t) - p_{\mathrm{ref}}(z)$, ...

Thermal equation of state:

$$p_{\mathrm{ref}} = \rho_{\mathrm{ref}}(RT)_{\mathrm{ref}} \; , \tag{3a}$$

$$\cancel{p'/p_{\mathrm{ref}}} = \rho'/\rho_{\mathrm{ref}} + (RT)'/(RT)_{\mathrm{ref}} + (\rho'/\rho_{\mathrm{ref}})\,(RT)'/(RT)_{\mathrm{ref}} \; , \tag{3b}$$

which can be written as

$$p_{\mathrm{ref}} = \rho RT \; . \tag{4}$$

The gas constant depends on the composition

$$R \equiv q_{\mathrm{d}}R_{\mathrm{d}} + q_{\mathrm{v}}R_{\mathrm{v}} = R_{\mathrm{d}}(1 + \epsilon_1 q_{\mathrm{v}}) \; , \tag{5}$$

where $\epsilon_1 \equiv R_{\mathrm{v}}/R_{\mathrm{d}} - 1 \approx 0.608$.

Anelastic Approximation

Decompose the thermodynamic state of a fluid particle into a reference state that describes a **hydrostatic base-state** atmosphere,

$$\nabla p_{\mathrm{ref}} = \rho_{\mathrm{ref}} \mathbf{g} \,, \tag{2}$$

and a deviation thereof, e.g., $\rho'(\mathbf{x},t) \equiv \rho(\mathbf{x},t) - \rho_{\mathrm{ref}}(z)$, $p'(\mathbf{x},t) \equiv p(\mathbf{x},t) - p_{\mathrm{ref}}(z)$, ...

Conservation equations:

$$\nabla\cdot\left[(\rho_{\mathrm{ref}} + \cancel{\rho'})\mathbf{v}\right] = \cancel{-\partial_t \rho_{\mathrm{ref}}} - \cancel{\partial_t \rho'} \,, \tag{5a}$$

$$(\rho_{\mathrm{ref}} + \cancel{\rho'})(\mathrm{D}\mathbf{v} + 2\boldsymbol{\Omega}\times\mathbf{v}) = -\nabla p' + \nabla\cdot\boldsymbol{\tau} + \rho'\mathbf{g} \tag{5b}$$

$$(\rho_{\mathrm{ref}} + \cancel{\rho'})\mathrm{D}(h + e_{\mathrm{p}} + \cancel{e_{\mathrm{k}}}) = -\nabla\cdot(\rho\mathbf{j}_h + \rho\mathbf{j}_r - \cancel{\boldsymbol{\tau}\cdot\mathbf{v}}) + \cancel{\partial_t p_{\mathrm{ref}}} + \cancel{\partial_t p'} \,, \tag{5c}$$

$$(\rho_{\mathrm{ref}} + \cancel{\rho'})\mathrm{D}q_{\mathrm{v}} = -\nabla\cdot(\rho\mathbf{j}_{\mathrm{v}}) \,, \tag{5d}$$

Anelastic Approximation

Decompose the thermodynamic state of a fluid particle into a reference state that describes a **hydro-static base-state** atmosphere,

$$\nabla p_{\mathrm{ref}} = \rho_{\mathrm{ref}} \mathbf{g} \,, \tag{2}$$

and a deviation thereof, e.g., $\rho'(\mathbf{x},t) \equiv \rho(\mathbf{x},t) - \rho_{\mathrm{ref}}(z)$, $p'(\mathbf{x},t) \equiv p(\mathbf{x},t) - p_{\mathrm{ref}}(z)$, ...

Notes:

1. Density variations are still key via the buoyancy force

$$b \equiv -g\rho'/\rho_{\mathrm{ref}} \approx (RT)'/(RT)_{\mathrm{ref}} \,. \tag{6}$$

2. **Boussinesq limit**:

   If the vertical displacement of the fluid particle is much smaller than the scale height ($\approx 8\ \mathrm{km}$), we can consider ρ_{ref} as constant. Often used in shallow ABLs of $1\ \mathrm{km}$ or less.

Energy Variable

Several options:

$$\rho \mathrm{D}e = \psi - \nabla\cdot(\rho\mathbf{j}_h + \rho\mathbf{j}_r) - p\nabla\cdot\mathbf{v} \ , \tag{7a}$$

$$\rho \mathrm{D}h = \psi - \nabla\cdot(\rho\mathbf{j}_h + \rho\mathbf{j}_r) + \mathrm{D}p \ , \tag{7b}$$

$$\rho T \mathrm{D}s = \psi - \nabla\cdot(\rho\mathbf{j}_h + \rho\mathbf{j}_r) \ . \tag{7c}$$

Multiplying the momentum equation by $\mathbf{v}$ and adding it to the enthalpy equation yields

$$\rho \mathrm{D}(h + e_\mathrm{p} + e_\mathrm{k}) = \partial_t p + \nabla\cdot(\mathbf{u}\cdot\boldsymbol{\tau} - \rho\mathbf{j}_h - \rho\mathbf{j}_r) \tag{8}$$

which, for low Mach numbers and slowly varying large-scale conditions, yields

$$\rho \mathrm{D}(h + e_\mathrm{p}) \simeq -\nabla\cdot(\rho\mathbf{j}_h + \rho\mathbf{j}_r) \ , \tag{9}$$

where $h_\mathrm{s} \equiv h + e_\mathrm{p}$ is the **static energy**.

We use either static energy or entropy (**potential temperature**), because they are conserved in isentropic (adiabatic and reversible) processes, e.g., frictionless adiabatic ascent or descent through the atmosphere, whereas temperature is not.

Summary of Governing Equations

Cloud-free conditions, Boussinesq limit:

$$\partial_t \mathbf{v} + \nabla\cdot(\mathbf{v}\otimes\mathbf{v}) + 2\Omega\mathbf{k}\times(\mathbf{v} - U_{\mathrm{g}}\mathbf{i}) = -\nabla\pi + \nu\nabla^2\mathbf{v} + b\mathbf{k} \tag{10a}$$

$$\nabla\cdot\mathbf{v} = 0 \tag{10b}$$

$$\partial_t h_{\mathrm{s}}' + \nabla\cdot(\mathbf{v}h_{\mathrm{s}}') = \kappa_h\nabla^2 h_{\mathrm{s}}' \tag{10c}$$

$$\partial_t q_{\mathrm{v}} + \nabla\cdot(\mathbf{v}q_{\mathrm{v}}) = \kappa_{\mathrm{v}}\nabla^2 q_{\mathrm{v}}\ , \tag{10d}$$

where

$$b \equiv -g\rho'/\rho_{\mathrm{ref}} \approx (RT)'/(RT)_{\mathrm{ref}} = \alpha_{\mathrm{s}} h_{\mathrm{s}}' + \alpha_{\mathrm{v}} q_{\mathrm{v}}\ . \tag{11}$$

For appropriate boundary conditions, and using the approximation $\kappa_h \approx \kappa_{\mathrm{v}}$, we can reduce the two scalar equations to just one

$$\partial_t b + \nabla\cdot(\mathbf{v}b) = \kappa\nabla^2 b\ . \tag{12}$$

(For typical atmospheric conditions, one finds $\kappa_h/\kappa_{\mathrm{v}} \approx 0.8$.)

Idealized Configurations (Idealized Boundary Conditions)

Flat surface and horizontal homogeneity in free atmosphere:

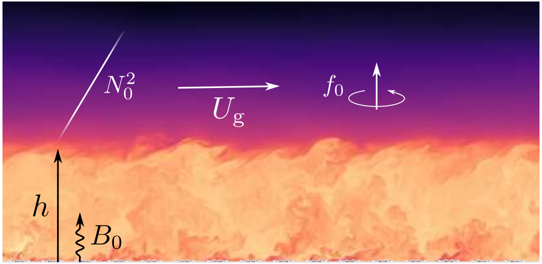

B_0	Surface buoyancy flux
N_0	Free-troposphere buoyancy frequency
U_g	Geostrophic wind
f_0	Coriolis parameter $(= 2\Omega \sin(\phi))$
h	Boundary-layer depth

Major control parameters:

Reynolds number | Richardson or Froude number | Rossby number

Not many, but very rich class of problems:

- Different types of buoyancy forcing: neutrally, stably or unstably stratified, surface heterogeneity...
- Unsteadiness: diurnal cycle, inertial oscillations, initial conditions.

Turbulence in the Atmospheric Boundary Layer

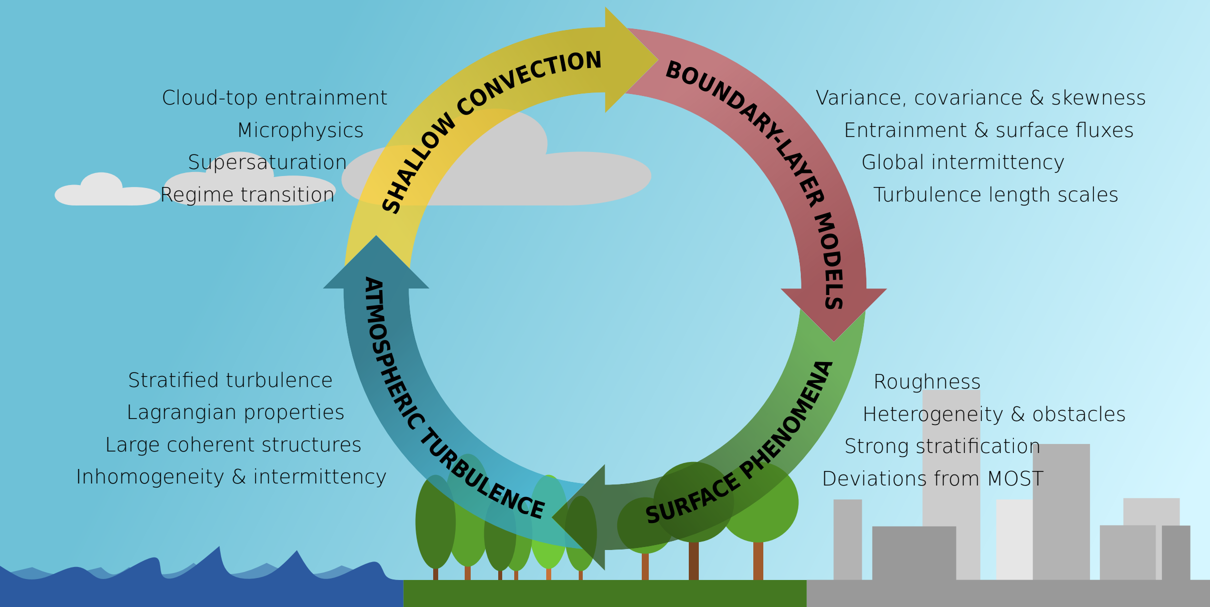

Contents

General problem

Find the mean horizontal velocity, $\langle u \rangle$, as a function of time, t, the distance from the surface, z, and free-troposphere and surface parameters, α_i:

$$\langle u \rangle = f(z\,, t\,, \alpha_{\mathrm{ft},i}, \alpha_{\mathrm{s},i}) \qquad (13)$$

$\langle \cdot \rangle$ indicates an ensemble average. The problem is split into subproblems.

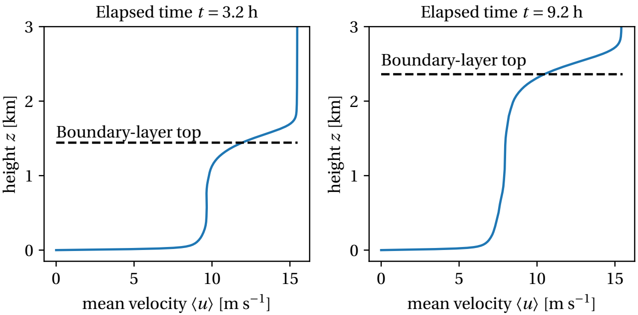

Figures adapted from Haghshenas and Mellado [2019].

Problem Statement: Find the Mean Velocity Near the Surface

General problem

Find the mean horizontal velocity, $\langle u \rangle$, as a function of time, t, the distance from the surface, z, and free-troposphere and surface parameters, α_i:

$$\langle u \rangle = f(z\,, t\,, \alpha_{\mathrm{ft},i}, \alpha_{\mathrm{s},i}) \qquad (13)$$

$\langle \cdot \rangle$ indicates an ensemble average. The problem is split into subproblems.

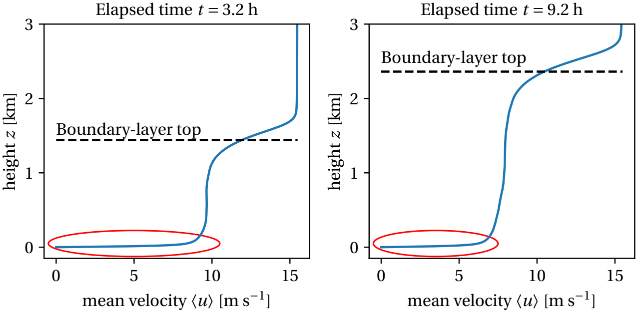

Figures adapted from Haghshenas and Mellado [2019].

Phenomenological Analysis: Large Scale Separation

Assumptions:

- The characteristic scale in the horizontal direction is much larger than the boundary-layer depth, h.
- $h \gg h_\mathrm{s}$, where h_s is a reference roughness-element height.

Consequences:

- Outer region: Far from the surface, we do not observe h_s nor surface parameters, $\alpha_{\mathrm{s},i}$.
- Inner region: Near the surface, we do not observe h nor free-troposphere parameters, $\alpha_{\mathrm{ft},i}$.

Phenomenological Analysis: Large Scale Separation

Assumptions:

- The characteristic scale in the horizontal direction is much larger than the boundary-layer depth, h.
- $h \gg h_\mathrm{s}$, where h_s is a reference roughness-element height.

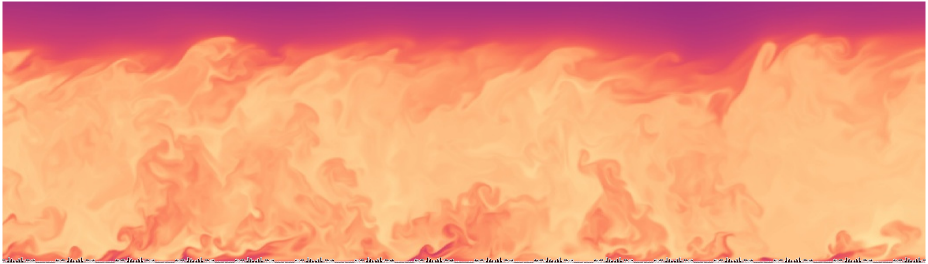

Consequences:

- Outer region: Far from the surface, we do not observe h_s nor surface parameters, $\alpha_{\mathrm{s},i}$.
- Inner region: Near the surface, we do not observe h nor free-troposphere parameters, $\alpha_{\mathrm{ft},i}$.

Phenomenological Analysis: Large Scale Separation

Assumptions:

- The characteristic scale in the horizontal direction is much larger than the boundary-layer depth, h.
- $h \gg h_\mathrm{s}$, where h_s is a reference roughness-element height.

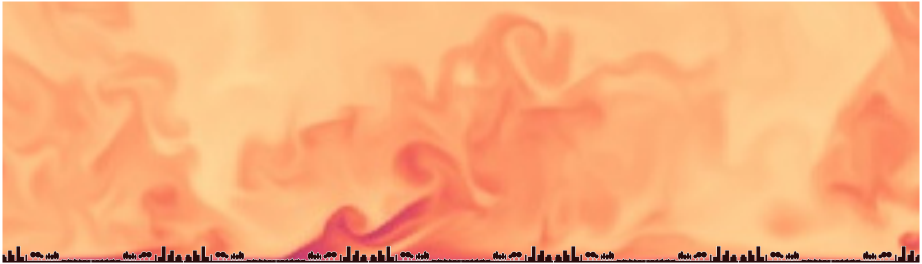

Consequences:

- Outer region: Far from the surface, we do not observe h_s nor surface parameters, $\alpha_{\mathrm{s},i}$.
- Inner region: Near the surface, we do not observe h nor free-troposphere parameters, $\alpha_{\mathrm{ft},i}$.

Overlap Region between Inner and Outer Regions

Because $h \gg h_\mathrm{s}$, the inner and outer regions overlap in an interval $h_\mathrm{s} \ll z \ll h$, where dimensional analysis leads to

$$\frac{z}{u_*}\frac{\partial\langle u\rangle}{\partial z} = \text{constant}\ . \tag{14}$$

The constant is written as k^{-1}, and k is the **von Kármán's constant**. It is universal and $k \approx 0.41$.

$$u_* \equiv \sqrt{\tau_\mathrm{s}/\rho} \tag{15}$$

is the **friction velocity**, where τ_s is the surface drag per unit of horizontal area. Typical values are $u_* \approx 0.15 - 0.70\ \mathrm{m\ s^{-1}}$.

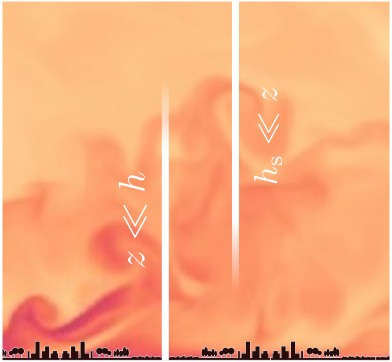

Logarithmic Law of the Wind Profile

Integration yields

$$\langle u \rangle = \frac{u_*}{k} \ln z + \text{constant} \,, \qquad (16)$$

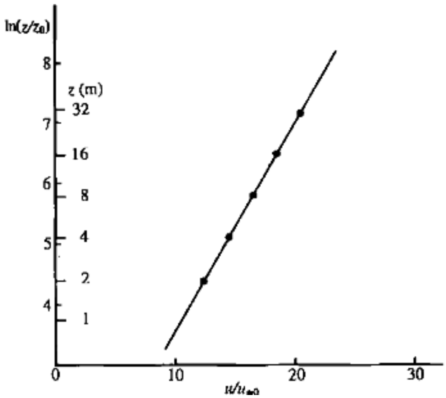

Figure 3.5 from Garratt [1992], 1971 Kansas experiment.

Logarithmic Law of the Wind Profile

Integration yields

$$\langle u \rangle = \frac{u_*}{k} \ln \frac{z}{z_0} \,, \qquad (16)$$

which is the logarithmic law. Measurements confirm it between $\approx 30\, z_0$ and $\approx 0.1\, h$, where h is the boundary-layer depth.

The parameter z_0 is the **roughness length**, an integration constant. It embeds the dependence of $\langle u \rangle$ on the surface properties, $z_0 = z_0(h_\mathrm{s}, \alpha_{\mathrm{s},i})$.

When $z_0 = z_0(h_\mathrm{s})$, z_0 is $\approx 10\%$ of the roughness element height: from millimeters for sand, snow, to meters for forests and urban areas.

Otherwise, obtaining $z_0 = z_0(h_\mathrm{s}, \alpha_{\mathrm{s},i})$ is a major challenge.

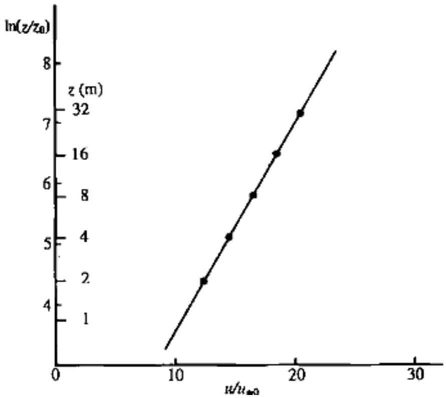

Figure 3.5 from Garratt [1992], 1971 Kansas experiment.

Effects of Static Stability: Monin-Obukhov Similarity Theory (MOST)

We retain the surface buoyancy flux B_0 as control parameter in addition to u_*. From dimensional analysis, one finds

$$\frac{kz}{u_*}\frac{\partial\langle u\rangle}{\partial z} = \phi(\zeta)\ , \qquad \zeta = z/L_{\mathrm{Ob}}\ , \tag{17}$$

where

$$L_{\mathrm{Ob}} = -\frac{u_*^3}{kB_0} \tag{18}$$

is the **Obukhov scale**. By construction, $\phi(0) = 1$, and for small magnitudes of ζ one can consider $\phi(\zeta) = 1 + \beta\zeta$ which leads to a logarithmic law plus corrections.

What is $\phi(\zeta)$ for strongly stable and strongly unstable conditions?

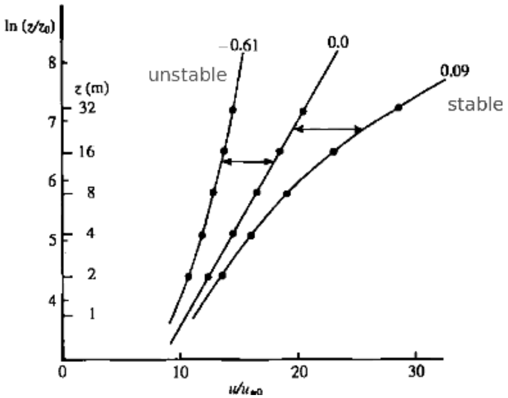

Obukhov [1946], Wyngaard [2010]. Figure 3.5 from Garratt [1992], 1971 Kansas experiment.

Deviations from Monin-Obukhov in Stable Conditions

1. Models artificially enhance diffusivity to reduce biases, which deteriorates boundary layer properties.
   Holtslag et al. [2013], Sandu et al. [2013]
2. Intermittency during turbulence collapse is particularly challenging.
   Mahrt [2014]

Near-surface enstrophy. Courtesy of Cedrick Ansorge, adapted from Ansorge [2019].

3. Now we can simulate it under control conditions: New opportunities for analysis.
   Flores and Riley [2011], Ansorge and Mellado [2014, 2016], Deusebio et al. [2014, 2015]

Deviations from Monin-Obukhov Similarity Theory in Unstable Conditions

Wyngaard Et al. 1971, Kansas field measurements.

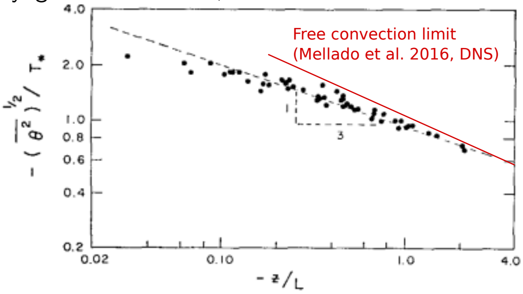

Fig. 7. Dimensionless rms temperature fluctuations under unstable conditions. The $-\frac{1}{3}$ slope is the local free convection prediction.

Maronga & Reuder 2017, LES

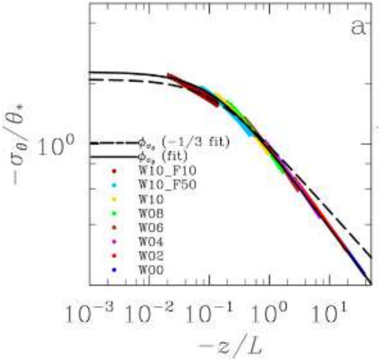

1. Temperature, moisture r.m.s. fall faster with height (an r.m.s. factor of 2 across the surface layer.)
2. Strong dependence of skewness on tropospheric conditions.
3. Relevant for cloud formation (fog), chemistry.

Caused by Outer Scales, Attributed to the Large Convective Cells

Near-surface vertical velocity: red, upwards; blue, downwards.

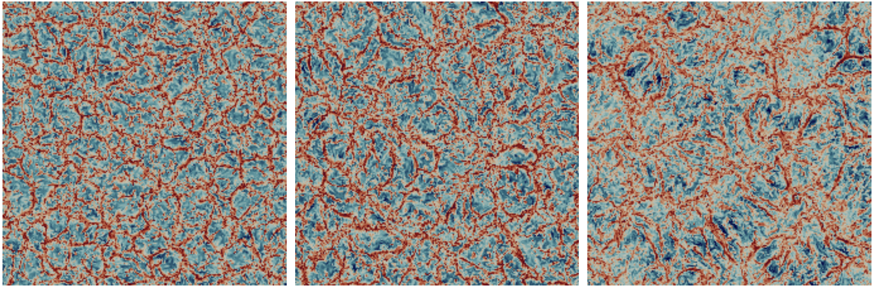

Increasing troposphere stratification or boundary-layer top cooling from left to right.

Hypothesis Testing

1. Shear effects in internal boundary layers parallel to the surface.
   Kraichnan [1962], Businger [1973], van Reeuwijk et al. [2008]
2. Large-scale downdrafts transport unmixed free-tropospheric air into the surface layer.
   de Bruin et al. [1993], Lohou et al. [2010], van de Boer et al. [2014]

Caused by Outer Scales, Attributed to the Large Convective Cells

Near-surface vertical velocity: red, upwards; blue, downwards.

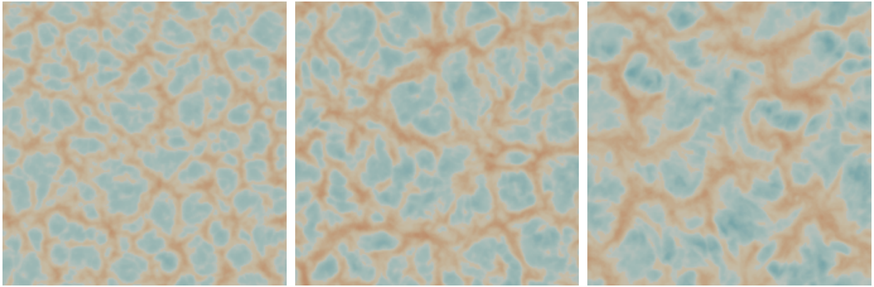

Increasing troposphere stratification or boundary-layer top cooling from left to right.

Hypothesis Testing

1. Shear effects in internal boundary layers parallel to the surface.
   Kraichnan [1962], Businger [1973], van Reeuwijk et al. [2008]
2. Large-scale downdrafts transport unmixed free-tropospheric air into the surface layer.
   de Bruin et al. [1993], Lohou et al. [2010], van de Boer et al. [2014]

Caused by Outer Scales, Attributed to the Large Convective Cells

Near-surface vertical velocity: red, upwards; blue, downwards.

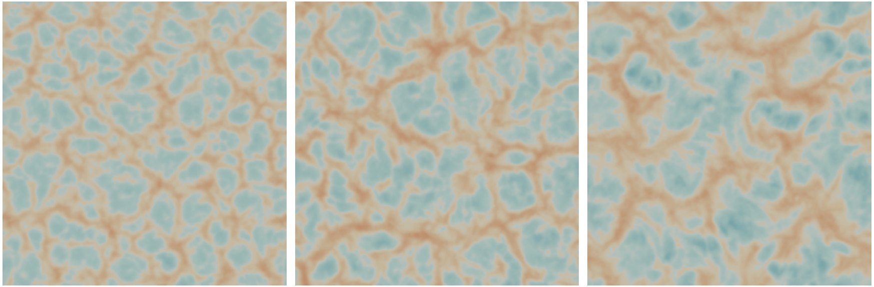

Increasing troposphere stratification or boundary-layer top cooling from left to right.

Hypothesis Testing

1. Shear effects in internal boundary layers parallel to the surface.
   Kraichnan [1962], Businger [1973], van Reeuwijk et al. [2008]
2. Large-scale downdrafts transport unmixed free-tropospheric air into the surface layer.
   de Bruin et al. [1993], Lohou et al. [2010], van de Boer et al. [2014]

Conditional analysis in downdrafts and updrafts falsify 2. hypothesis [Fodor et al., 2019].

Large coherent motions affect the surface layer, but how?

Surface Heterogeneity Affect Large Convective Cells

1. Plume-bubble regime transitions over cities [Omidvar et al., 2020].

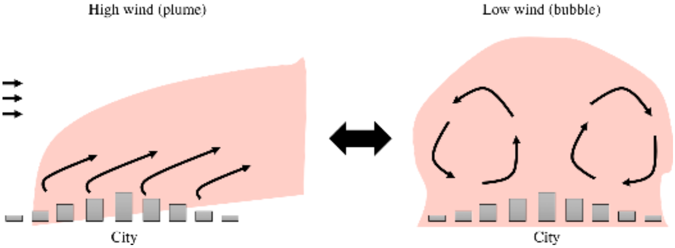

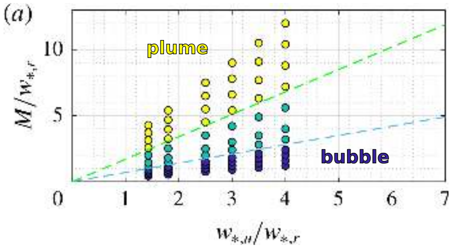

Surface Heterogeneity Affect Large Convective Cells

1. Plume-bubble regime transitions over cities [Omidvar et al., 2020].
2. Roughness heterogeneity [Vanderwel et al., 2019].

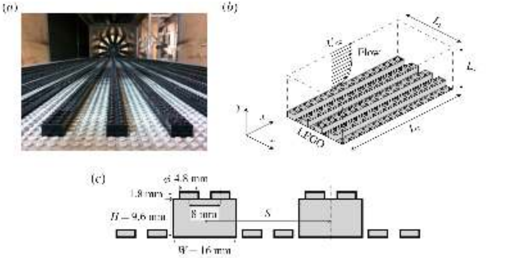

FIGURE 1. (Colour online) (a) Photograph of the experiment and (b) schematic of the numerical set-up with (c) dimensions of the considered elements and their distribution.

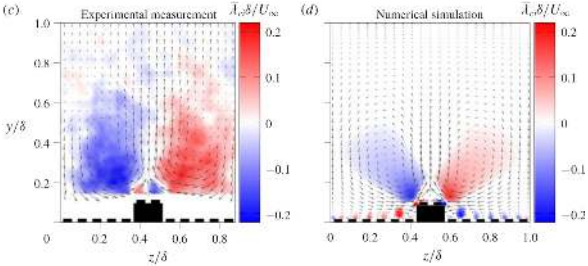

FIGURE 2. (Colour online) Time-averaged velocity and signed swirling strength.

Roughness-induced large coherent motions interact with convectively induced ones.

Immersed boundary methods gives us the opportunity to study these problems numerically.

Surface Phenomena

Open Issues:

1. Flux-gradient relationships, near-surface covariances and skewness.
2. Their dependence on stability, surface heterogeneity, mesoscale conditions.
3. Role of large coherent structures.
4. Transients (turbulence collapse, internal boundary layers, bubble-plume regimes), deviations from quasi-steady conditions.

Contents

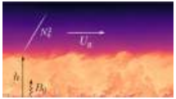

Bulk (Integral) Models in Unstable Conditions

Bulk (Integral) Models in Unstable Conditions

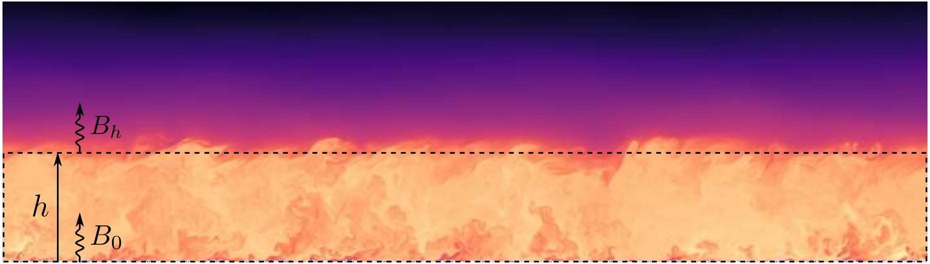

- h is the boundary-layer depth (unknown).
- B_0 is the surface buoyancy flux.
- B_h is the entrainment buoyancy flux (unknown).

Problem Statement: Find the Mean Velocity inside the ABL

General problem

Find the mean horizontal velocity, $\langle u \rangle$, as a function of time, t, the distance from the surface, z, and free-troposphere and surface parameters, α_i:

$$\langle u \rangle = f(z\,, t\,, \alpha_{\mathrm{ft},i}, \alpha_{\mathrm{s},i}) \qquad (19)$$

$\langle \cdot \rangle$ indicates an ensemble average. The problem is split into subproblems.

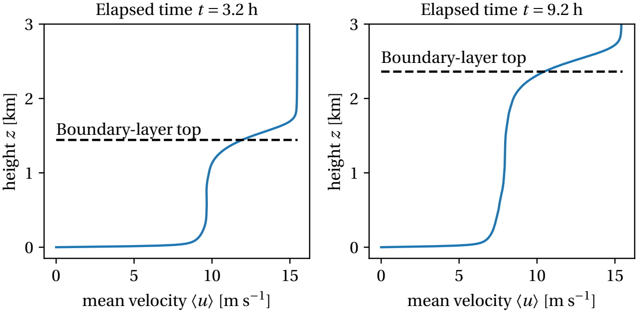

Entrainment in Unstable Conditions

1. Entrainment fluxes determine boundary-layer depth and derived properties, like mean values and fluctuations intensities, major variables in boundary-layer schemes.

   It is difficult to extrapolate field measurements to different environmental conditions.

   Mahrt [1991], Wulfmeyer et al. [2016], Davy and Esau [2016]

Entrainment in Unstable Conditions

1. Entrainment fluxes determine boundary-layer depth and derived properties, like mean values and fluctuations intensities, major variables in boundary-layer schemes.

   It is difficult to extrapolate field measurements to different environmental conditions.

   Mahrt [1991], Wulfmeyer et al. [2016], Davy and Esau [2016]

2. Entrainment-zone properties are themselves important, for instance, moisture and temperature statistics for cloud formation.

   Uncertainties are associated with small scales.

   Fedorovich et al. [2004], Conzemius and Fedorovich [2007], Pino and de Arellano [2008]

The Ozmidov Length Scale Characterizes the Entrainment Zone

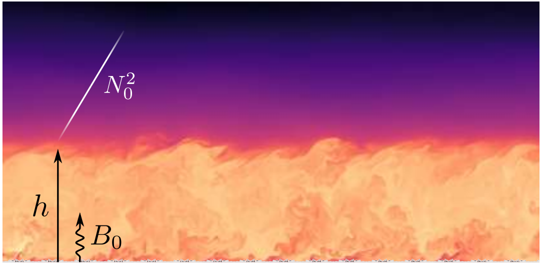

h	Boundary-layer depth
B_0	Surface buoyancy flux
N_0	Free-troposphere buoyancy frequency

In the limit of free convection, the system depends only on the Reynolds number and h/L_0, where

$$L_0 \equiv (B_0/N_0^3)^{1/2}$$

is an Ozmidov scale. It provides a reference entrainment-zone thickness and thereby other reference properties in the entrainment zone.

Typical atmospheric midday values over land: $L_0 \approx 20{-}200\,\mathrm{m}$ $(h/L_0 \approx 5{-}50)$. **We need meter-scale resolution in the entrainment zone.**

Dougherty [1961], Ozmidov [1965], Garcia and Mellado [2014]

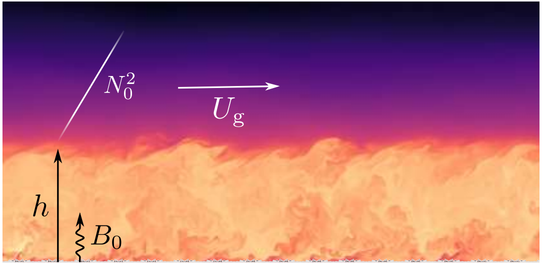

h	Boundary-layer depth
B_0	Surface buoyancy flux
N_0	Free-troposphere buoyancy frequency
U_{g}	Geostrophic wind

In addition to the Reynolds number and h/L_0, we have the Froude number

$$\mathrm{Fr}_0 \equiv U_{\mathrm{g}}/(N_0 L_0)$$

where L_0 is the reference Ozmidov scale.

Typical atmospheric midday values over land $\mathrm{Fr}_0 \approx 0 - 35$, which corresponds to $U_{\mathrm{g}} \approx 10 - 15 \ \mathrm{m\ s^{-1}}$.

Wind Shear Adds an Additional Local Scale in the Entrainment Zone

We have enough accuracy and resolution to differentiate scales in the entrainment zone. In particular, the buoyancy flux scales with a local length and not the boundary-layer depth.

From the integral analysis of the TKE budget, one finds the local length

$$\Delta z_\mathrm{i} \approx 0.25\, h \sqrt{1 + 4.8 \left(\frac{\Delta u}{N_0 h} \right)^2} \,,$$

where

$$\Delta u \equiv \| \mathbf{U}_\mathrm{g} - \mathbf{u}_\mathrm{ml} \|$$

is the velocity increment across the entrainment zone.

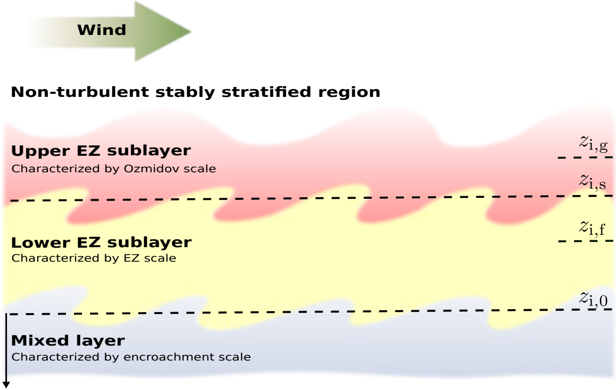

Haghshenas and Mellado [2019]

Use for Parametrizations of Boundary-Layer Properties

For instance, reference heights in the entrainment zone:

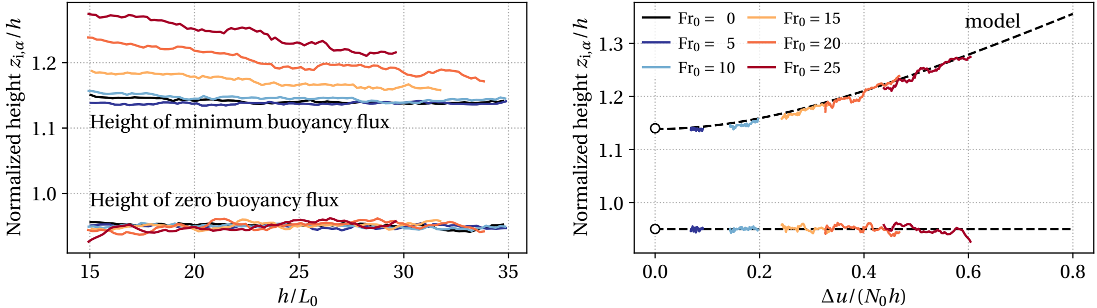

Advantages:

1. Shear effects are quantified in terms of Δu, the velocity increment across the entrainment zone, which is more robust than a pointwise quantity like the gradient at one point.
2. Eliminates the singularity at finite wind speed that was found in previous bulk models.

Add Coriolis Effects to the Problem

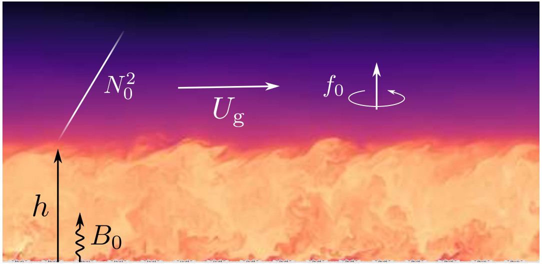

h	Boundary-layer depth
B_0	Surface buoyancy flux
N_0	Free-troposphere buoyancy frequency
U_g	Geostrophic wind
f_0	Coriolis parameter

In addition to the Reynolds number, h/L_0, and the Froude number, we have the Rossby number

$$\mathrm{Ro}_0 \equiv N_0/f_0 \ .$$

Typical atmospheric values are $\mathrm{Ro}_0 \approx 40 - \infty$.

Scaling Laws Are Approximately Independent of Coriolis Effects

1. The center of the mixed layer marks the height of wind veering.

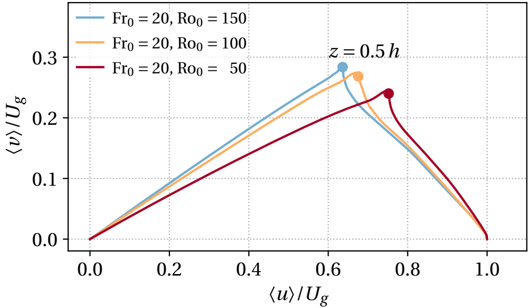

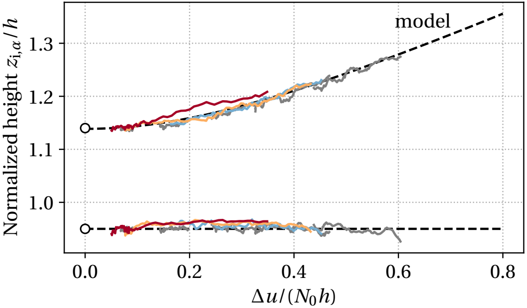

2. We can still use the same definition of velocity increment across the entrainment zone

$$\Delta u \equiv \left\| \mathbf{U}_\mathrm{g} - \mathbf{u}_\mathrm{ml} \right\| .$$

3. Same scaling laws hold: **One single curve embeds the dependence on $\{h,\, B_0,\, N_0,\, U_\mathrm{g},\, f_0\}$.**

Scaling Laws Are Approximately Independent of Coriolis Effects

1. The center of the mixed layer marks the height of wind veering.

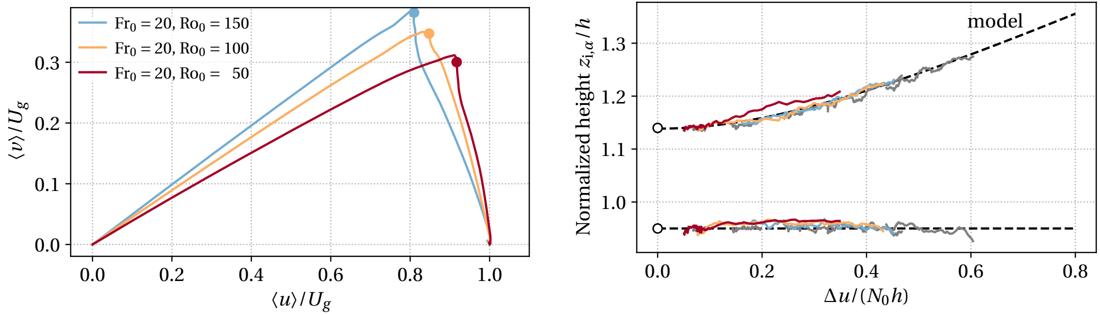

2. We can still use the same definition of velocity increment across the entrainment zone

$$\Delta u \equiv \|\mathbf{U}_\mathrm{g} - \mathbf{u}_\mathrm{ml}\| \; .$$

3. Same scaling laws hold: **One single curve embeds the dependence on $\{h,\, B_0,\, N_0,\, U_\mathrm{g},\, f_0\}$.**

Scaling Laws Are Approximately Independent of Coriolis Effects

1. The center of the mixed layer marks the height of wind veering.

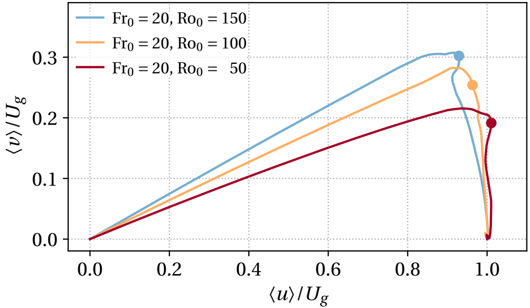

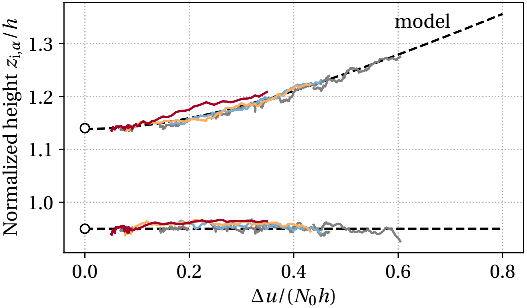

2. We can still use the same definition of velocity increment across the entrainment zone

$$\Delta u \equiv \|\mathbf{U}_\mathrm{g} - \mathbf{u}_\mathrm{ml}\| \,.$$

3. Same scaling laws hold: **One single curve embeds the dependence on $\{h,\, B_0,\, N_0,\, U_\mathrm{g},\, f_0\}$.**

Open Issues:

1. Entrainment fluxes.
2. Entrainment variance and skewness. Moisture statistics and cloud formation.
3. Microscale-mesoscale interaction: Dependence on mesoscale variability in atmosphere and surface.
4. Transients (diurnal cycle, horizontal advection), deviations from quasi-steady conditions.

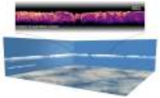

Contents

Prevalent Regimes of Maritime Convection in the Tropics and Subtropics

Following the trades in a Lagrangian framework, we sample three main regimes: stratocumulus, shallow cumulus and deep convection:

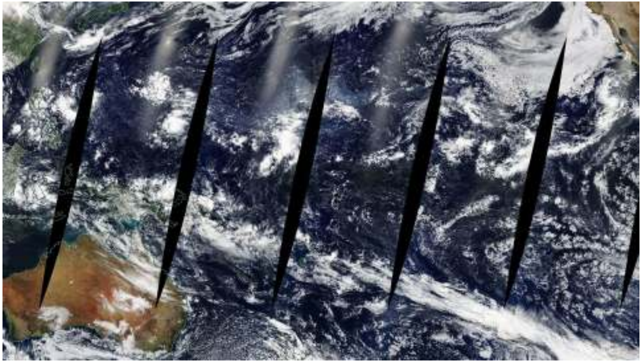

NASA Worldview June 25th, 2018

They are structural components of the general circulation of the atmosphere and they highlight the interaction of convection and mixing with radiation, organization and precipitation.

Prevalent Regimes of Maritime Convection in the Tropics and Subtropics

Following the trades in a Lagrangian framework, we sample three main regimes: stratocumulus, shallow cumulus and deep convection:

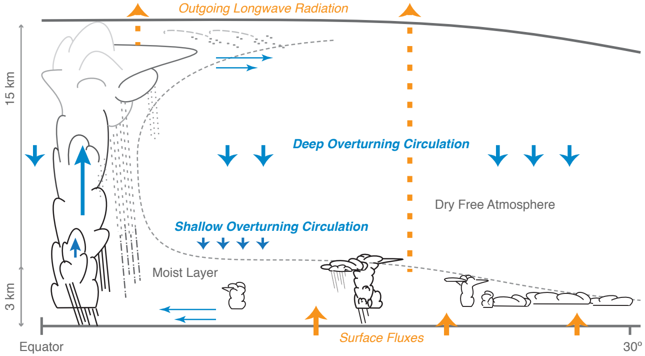

Courtesy of Bjorn Stevens. Adapted from Stevens [2005].

They are structural components of the general circulation of the atmosphere and they highlight the interaction of convection and mixing with radiation, organization and precipitation.

Stratocumulus

Stratocumulus are stratiform cloud systems that form at the top of shallow ABLs.

NASA Worldview June 25th, 2018

Stratocumulus

Stratocumulus are stratiform cloud systems that form at the top of shallow ABLs.

North Atlantic. Courtesy of Cedrick Ansorge.

Importance and Challenges

1. Because of their radiative properties, a $4-5\%$ increase in stratocumulus area coverage could offset a $2\ \mathrm{K}$ warming.

   But characterizing their sensitivity to environmental conditions remains a challenge.

   Randall [1980], Lilly [1968], Wood [2012]

2. When appropriately tuned, LES shows skill in process studies and climate change sensitivity studies, but quantitative prediction remains difficult.

   This difficulty is mainly attributed to an inadequate representation of cloud-top mixing.

   Bretherton et al. [1999], Stevens et al. [2005], Sherwood et al. [2014]

Mixing: Need For Meter- and Submeter-Scale Resolution at the Cloud Top

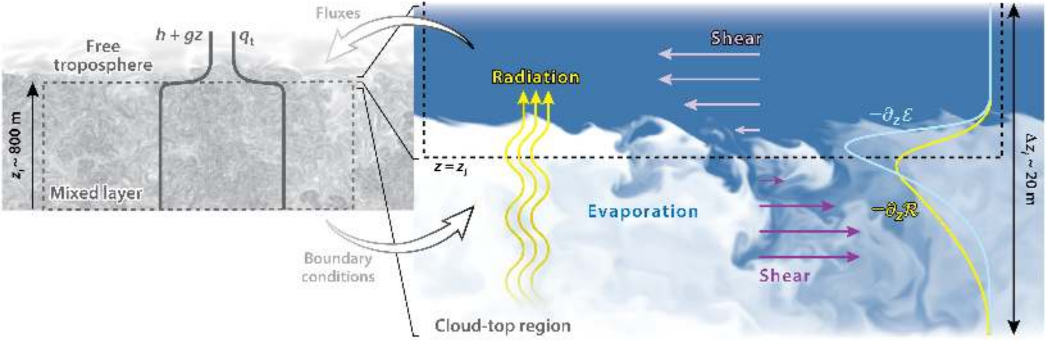

We need to represent the Ozmidov scale to reach the inertial range of the turbulence cascade:

$$L_{\mathrm{Oz}} \equiv (\varepsilon / N^3)^{1/2} \ .$$

Observational and numerical studies find $L_{\mathrm{Oz}} \simeq 0.3 - 4\ \mathrm{m}$, depending on environmental conditions.

Direct Numerical Simulations of Stratocumulus-Topped Boundary Layer

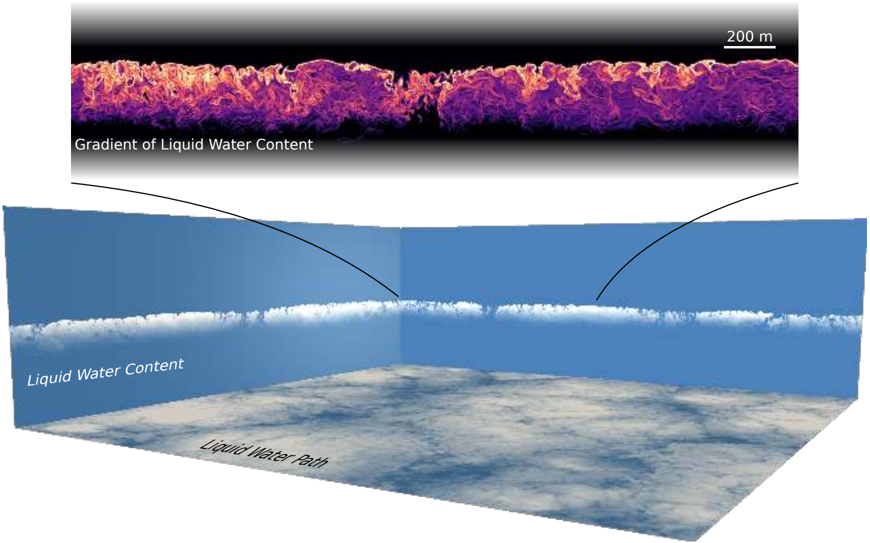

Governing Equations for DNS in Eulerian Framework

Disperse and dilute multi-phase flow (liquid volume fraction 10^{-6}) with small Stokes numbers ($< 10^{-2}$) and moderate settling numbers (≈ 0.5).

Anelastic approximation to Navier-Stokes equations:

$$\begin{aligned}
\text{enthalpy} \quad & \rho_{\mathrm{ref}} \mathrm{D}_t h = \nabla\cdot[\rho\kappa_h \nabla h - \rho\mathbf{j}_\mu (h_\ell - h)] - \nabla\cdot(\rho\mathbf{j}_\mathrm{r}) \ , \\
\text{total water} \quad & \rho_{\mathrm{ref}} \mathrm{D}_t q_\mathrm{t} = \nabla\cdot[\rho\kappa_\mathrm{v} \nabla q_\mathrm{t} - \rho\mathbf{j}_\mu (1 - q_\mathrm{t})] \ , \\
\text{liquid water} \quad & \rho_{\mathrm{ref}} \mathrm{D}_t q_\ell = \nabla\cdot[\rho\kappa_\mathrm{v} \nabla q_\ell - \rho\mathbf{j}_\mu (1 - q_\ell)] + (\partial_t \rho q_\ell)_{\mathsf{con}} \ .
\end{aligned}$$

Cloud processes to be modeled:

1. Radiative flux $\rho\mathbf{j}_\mathrm{r}$.
2. Rate of phase change $(\partial_t \rho q_\ell)_{\mathsf{con}}$: Latent heat effects.
3. Transport flux $\rho\mathbf{j}_\mu$: Droplet sedimentation.

Formulation of the Condensate Phase

1. Lagrangian microphysics.
   Accurate but expensive because typical cloud droplet number densities are $100-1000\,\mathrm{cm}^{-3}$. Current development of super-droplet approach.
2. Spectral bin microphysics.
   Modeling of the evolution equation for the droplet-size distribution. Accurate but also very expensive because the representation of the droplet size adds another dimension.
3. Bulk microphysics.
   Less accurate but cheaper because the droplet size distribution is assumed and only a few moments are represented.

Shaw [2003], Shima et al. [2009], Grabowski and Wang [2013], Khain et al. [2015]

Reaching Grid-Spacing Independence in DNS (Reynolds Number Similarity)

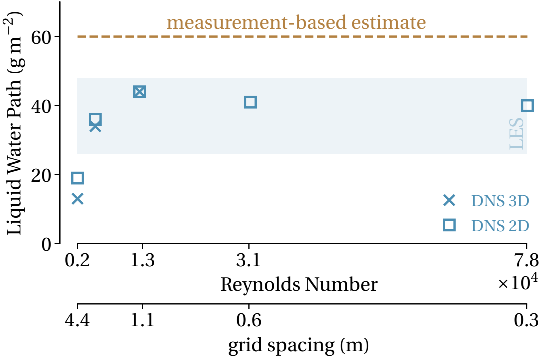

Grid spacings ≈ 1 m reproduce the central distribution of LES models (Stevens et al., 2005), $\approx 70\%$ of measured LWP, **without tuning**.

We can distinguish between biases due to mixing and biases due to misrepresentation of other processes.

Microphysics: Need for Submeter-Scale Resolution at the Cloud Top

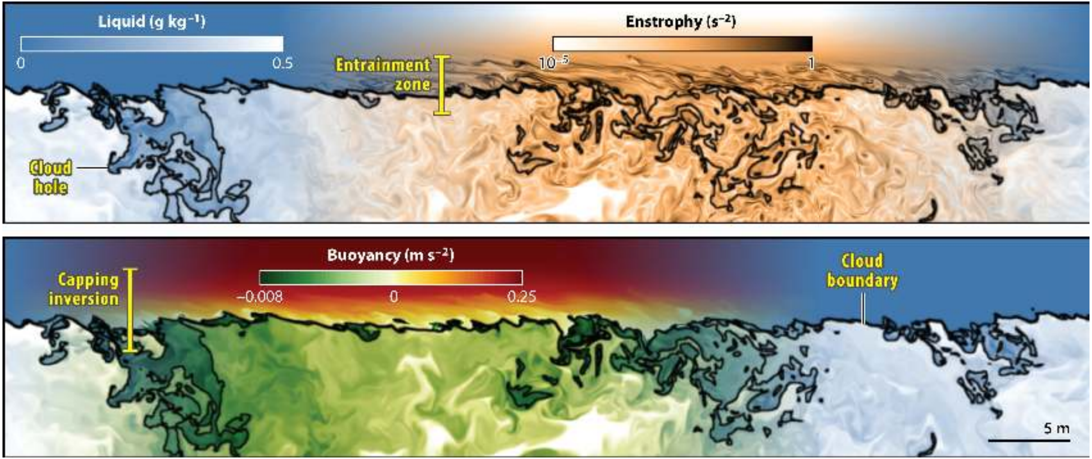

Droplet Sedimentation

Take same microphysics model as in LES and reduce grid spacing by a factor of 10.
Do we see the same?

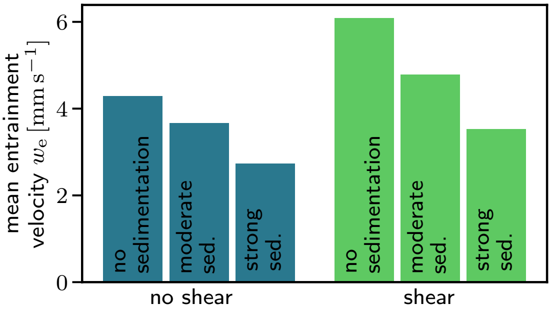

Almost 50% reduction of w_e, 2–3 times larger than previously reported.

The reason is that turbulence models are often down-gradient, which artificially enhances the liquid-water flux upwards, and this masks droplet sedimentation downwards.

Shallow Convection (Cloud-Turbulence Interaction)

Open issues:

1. Mixing plus micro-physics (sedimentation, phase-relaxation time, droplet-size distribution).
2. Supersaturation and aerosols in the entrainment zone (PDF tails)
3. Air-sea interaction: surface fluxes, waves.
4. Role of large coherent structures, open-closed cells, Sc-Cu transition, convective organization.
5. Microscale-mesoscale interaction: Dependence on mesoscale variability in atmosphere and ocean.
6. Transients (open-closed cells, Sc-Cu transition), deviations from quasi-steady conditions.
7. Mixed-phase clouds instead of only warm clouds.

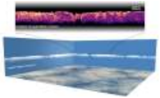

Contents

Turbulence in the Atmospheric Boundary Layer: Challenges

Multiscale | Multiphysics | Variability | Data

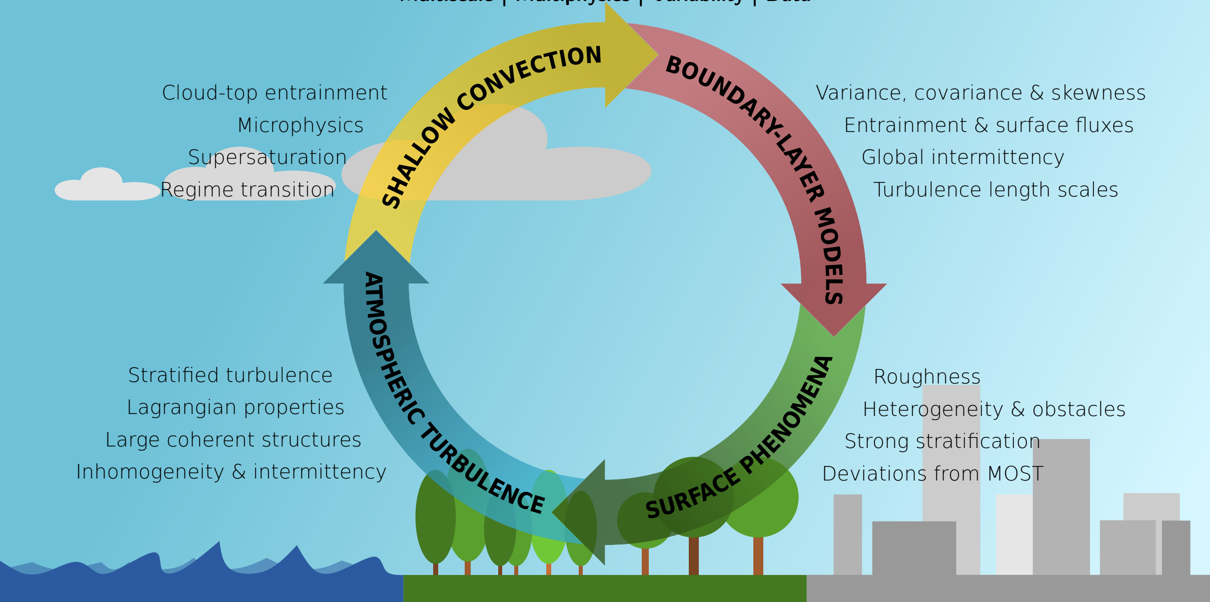

Thanks to high resolution, we have the opportunity to break 50-year-old deadlocks and get ready for kilometer-scale resolution in global models.

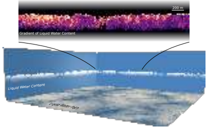

Direct numerical simulation reduces the uncertainty introduced by turbulence models, which clarifies the role of other phenomena.

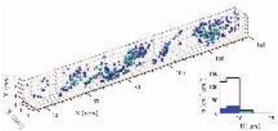

Synergy with field and laboratory to assess reduced complexity, unmatched non-dimensional numbers, and constrained variability in model studies.

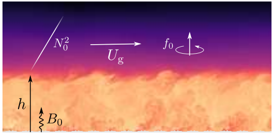

Control and systematic studies (dimensional analysis) of process interaction, hypothesis testing, microscale-mesoscale interaction for parametrizations.

First and third figures from Stevens and et. al. [2019] and Beals et al. [2015].

References and Further Reading I

C. Ansorge. Scale dependence of atmosphere-surface coupling through similarity theory. *Boundary-Layer Meteorol.*, 170:1–27, 2019.

C. Ansorge and J. P. Mellado. Global intermittency and collapsing turbulence in the stratified planetary boundary layer. *Boundary-Layer Meteorol.*, 153:89–116, 2014.

C. Ansorge and J. P. Mellado. Analysis of external and global intermittency in the logarithmic layer of Ekman flow. *J. Fluid Mech.*, 805:611–635, 2016.

P. R. Bannon. On the anelastic approximation for a compressible atmosphere. *J. Atmos. Sci.*, 53:3618–3628, 1996.

M. J. Beals, J. P. Fugal, R. A. Shaw, J. Lu, S. M. Spuler, and J. L. Stith. Holographic measurements of inhomogeneous cloud mixing at the centimeter scale. *Science*, 350:87–90, 2015.

C. S. Bretherton, M. K. Macvean, P. Bechtold, A. Chlond, W. R. Cotton, J. Cuxart, H. Cuijpers, M. Khairoutdinov, B. Kosovic, D. Lewellen, C.-H. Moeng, P. Siebesma, B. Stevens, D. E. Stevens, I. Sykes, and M. C. Wyant. An intercomparison of radiatively driven entrainment and turbulence in a smoke cloud, as simulated by different numerical models. *Q. J. Roy. Meteorol. Soc.*, 125:391–423, 1999.

J. A. Businger. A note on free convection. *Boundary-Layer Meteorol.*, 4:323–326, 1973.

R. Conzemius and E. Fedorovich. Bulk models in the sheared convective boundary layer: Evaluation through large eddy simulations. *J. Atmos. Sci.*, 64:786–807, 2007.

Richard Davy and Igor Esau. Differences in the efficacy of climate forcings explained by variations in atmospheric boundary layer depth. *Nature Communications*, 7, 2016.

H. de Bruin, W. Kohsiek, and B. van den Hurk. A verification of some methods to determine the fluxes of momentum, sensible heat, and water vapour using standard deviation and structure parameter of scalar meteorological quantities. *Boundary-Layer Meteorol.*, 63:231–257, 1993.

A. de Lozar and J. P. Mellado. Direct numerical simulations of a smoke cloud-top mixing layer as a model for stratocumuli. *J. Atmos. Sci.*, 70:2356–2375, 2013.

E. Deusebio, G. Brethouwer P. Schlatter, and E. Lindborg. A numerical study of the unstratified and stratified Ekman layer. *J. Fluid Mech.*, 755:672–704, 2014.

E. Deusebio, C. P. Caulfield, and J. R. Taylor. The intermittency boundary in stratified plane couette flow. *J. Fluid Mech.*, 781:298–329, 2015.

J. P. Dougherty. The anisotropy of turbulence at the meteor level. *J. Atmos. Terr. Phys.*, 21:210–213, 1961.

E. Fedorovich, R. Conzemius, and D. Mironov. Convective entrainment into a shear-free linearly stratified atmosphere: bulk models reevaluated through large-eddy simulation. *J. Atmos. Sci.*, 61:281–295, 2004.

O. Flores and J.J. Riley. Analysis of turbulence collapse in the stably stratified surface layer using direct numerical simulation. *Boundary-Layer Meteorol.*, 139:241–259, 2011.

K. Fodor, J. P. Mellado, and M. Wilczek. On the role of large-scale updrafts and downdrafts in deviations from Monin-Obukhov similarity theory in free convection. *Boundary-Layer Meteorol.*, 172:371–396, 2019. doi: 10.1007/s10546-019-00454-3.

J. R. Garcia and J. P. Mellado. The two-layer structure of the entrainment zone in the convective boundary layer. *J. Atmos. Sci.*, 71:1935–1955, 2014.

J. R. Garratt. *The Atmospheric Boundary Layer.* Cambridge University Press, 316 pp, 1992.

W. W. Grabowski and L.-P. Wang. Growth of cloud droplets in a turbulent environment. *Annu. Rev. Fluid Mech.*, 45:293–324, 2013.

A. Haghshenas and J. P. Mellado. Characterization of wind-shear effects on entrainment in a convective boundary layer. *J. Fluid Mech.*, 858:145–183, 2019.

A.A.M. Holtslag, G. Svensson, P. Baas, S. Basu, B. Beare, A.C.M. Beljaars, F.C. Bosveld, J. Cuxart, J. Lindvall, G.J. Steeneveld, M. Tjernström, and B.J.H. van de Wiel. Stable atmopsheric boundary layers and diurnal cycles. *Bull. Amer. Meteor. Soc.*, 94:1691–1706, 2013.

References and Further Reading II

A. Khain, K. D. Beheng, A. Heymsfield, A. Korolev, S. O. Krichak, Z. Levin, M. Pinsky, V. Phillips, T. Prabhakaran, A. Teller, S. C. van den Heever, and J.-I. Yano. Representation of microphysical processes in cloud-resolving models: Spectral (bin) microphysics versus bulk parameterization. *Rev. Geophys.*, 53:247–322, 2015.

R. Kraichnan. Turbulent thermal convection at an arbitrary Prandtl number. *Phys. Fluids*, 5(11):1374–1389, 1962.

Margaret A. LeMone, Wayne M. Angevine, Christopher S. Bretherton, Fei Chen, Jimy Dudhia, Evgeni Fedorovich, Kristina B. Katsaros, Donald H. Lenschow, Larry Mahrt, Edward G. Patton, Jielun Sun, Michael Tjernström, and Jeffrey Weil. 100 years of progress in boundary layer meteorology. *Meteorological Monographs*, 59:9.1–9.85, 2019. doi: 10.1175/AMSMONOGRAPHS-D-18-0013.1.

D. K. Lilly. Models of cloud-topped mixed layers under strong inversion. *Q. J. Roy. Meteorol. Soc.*, 94:292–309, 1968.

F. Lohou, M. Lothon, P Durand, and D Serça. Impact of boundary-layer processes on near-surface turbulence within the west african monsoon. *Boundary-Layer Meteorol.*, 136:1–23, 2010.

L. Mahrt. Boundary-layer moisture regimes. *Boundary-Layer Meteorol.*, 152:151–176, 1991.

L. Mahrt. Stably stratified atmospheric boundary layers. *Annu. Rev. Fluid Mech.*, 46:23–45, 2014.

J. P. Mellado. Cloud-top entrainment in stratocumulus clouds. *Annu. Rev. Fluid Mech.*, 41:145–169, 2017.

J. P. Mellado, C. S. Bretherton, B. Stevens, and M. C. Wyant. DNS and LES of stratocumulus: Better together. *J. Adv. Model. Earth Syst.*, 10:1421–1438, 2018.

A. M. Obukhov. Turbulence in an atmosphere with a non-uniform temperature. *Tr. Inst. Teo. Geofiz. Akad. Nauk. SSSR*, 1:95–115, 1946. In Russian, English trans.: 1971 *Boundary-Layer Meteorol.* **2**, 7–29.

H. Omidvar, E. Bou-Zeid, Q. Li, J. P. Mellado, and P. Klein. Plume or bubble? mixed-convection flow regimes and city-scale circulations. *J. Fluid Mech.*, 897(A5):1–27, 2020.

R. V. Ozmidov. On the turbulent exchange in a stably stratified ocean. *Izv., Atmospheric and Oceanic Physics Series*, 1:853–860, 1965.

D. Pino and J. V. G. de Arellano. Effects of shear in the convective boundary layer: analysis of the turbulent kinetic energy budget. *Acta Geophysica*, 56:167–193, 2008.

D. A. Randall. Conditional instability of the first kind upside-down. *J. Atmos. Sci.*, 37:125–130, 1980.

C. Reynolds, K. Williams, and A. Zadra. Wgne systematic error survey results summary. Technical report, World Climate Research Programme, 2019.

I. Sandu, A. Beljaars, P. Bechtold, T. Mauritsen, and G. Balsamo. Why is it so difficult to represent stably stratified conditions in numerical weather prediction (NWP) models? *J. Adv. Model. Earth Syst.*, 5(2):117–133, 2013.

B. Schulz and J. P. Mellado. Competing effects of wind shear and droplet sedimentation at stratocumulus tops. *J. Adv. Model. Earth Syst.*, 2019. doi: doi:10.1029/2019MS001617.

R. A. Shaw. Particle-turbulence interactions in atmospheric clouds. *Annu. Rev. Fluid Mech.*, 35:183–227, 2003.

S. C. Sherwood, S. Bony, and J.-L. Dufresne. Spread in model climate sensitivity traced to atmospheric convective mixing. *Nature*, 505:37–42, 2014.

S. Shima, K. Kusano, A. Kawano, T. Sugiyama, and S. Kawahara. The super-droplet method for the numerical simulation of clouds and precipitation: a particle-based and probabilistic microphysics model coupled with a non-hydrostatic model. *Q. J. Roy. Meteorol. Soc.*, 135:1307–1320, 2009.

B. Stevens. Atmospheric moist convection. *Annu. Rev. Earth Planet. Sci.*, 33:605–643, 2005.

B. Stevens and et. al. Dyamond: the dynamics of the atmospheric general circulation modeled on non-hydrostatic domains. *Progress in Earth and Planetary Science*, 6(61):1–17, 2019.

References and Further Reading III

B. Stevens, C.-H. Moeng, A. S. Ackerman, C. S. Bretherton, A. Chlond, S. de Roode, J. Edwards, J.-C. Golaz, H. Jiang, M. Khairoutdinov, M. P. Kirkpatrick, D. C. Lewellen, A. Lock, F. Müller, D. E. Stevens, E. Whelan, and P. Zhu. Evaluation of large-eddy simulations via observations of nocturnal marine stratocumulus. *Mon. Wea. Rev.*, 133:1443–1462, 2005.

A. van de Boer, A. F. Moene, A. Graf, S. Schüttemeyer, and C. Simmer. Detection of entrainment influences on surface-layer measurements and extension of Monin-Obukhov similarity theory. *Boundary-Layer Meteorol.*, 152:19–44, 2014.

M. van Reeuwijk, H. J. J. Jonker, and K. Hanjalić. Wind and boundary layers in Rayleigh-Bénard convection. I. Analysis and modeling. *Phys. Rev. E*, 77(036311):1–15, 2008.

C. Vanderwel, A. Stroh, J. Kriegseis, B. Frohnapfel, and B. Ganapathisubramani. The instantaneous structure of secondary flows in turbulent boundary layers. *J. Fluid Mech.*, 862:845–870, 2019. doi: 10.1017/jfm.2018.955.

J. M. Wallace and P. V. Hobbs. *Atmospheric Science*. Elsevier 483 pp, second edition, 2006.

R. Wood. Stratocumulus clouds. *Mon. Wea. Rev.*, 140:2373–2423, 2012.

V. Wulfmeyer, S. K. Muppa, A. Behrendt, E. Hammann, F. Späth, Z. Sorbjan, D. Turner, and R. M. Hardesty. Determination of convective boundary layer entrainment fluxes, dissipation rates, and the molecular destruction of variances: Theoretical description and a strategy for its confirmation with a novel Lidar system synergy. *J. Atmos. Sci.*, 73:667–692, 2016.

J. C. Wyngaard. *Turbulence in the Atmosphere*. Cambridge University Press, 393 pp, 2010.